



# The $3 \times 120^\circ$ rotary mechanism of *Paracoccus denitrificans* $F_1$ -ATPase is different from that of the bacterial and mitochondrial $F_1$ -ATPases

Maríel Zarco-Zavala<sup>a,1</sup> , Ryo Watanabe<sup>a</sup>, Duncan G. G. McMillan<sup>b</sup> , Toshiharu Suzuki<sup>c</sup>, Hiroshi Ueno<sup>a</sup> , Francisco Mendoza-Hoffmann<sup>d</sup>, José J. García-Trejo<sup>d,1</sup>, and Hiroyuki Noji<sup>a,1</sup>

<sup>a</sup>Department of Applied Chemistry, Graduate School of Engineering, The University of Tokyo, 113-8656 Tokyo, Japan; <sup>b</sup>Department of Biotechnology, Delft University of Technology, 2629 HZ Delft, the Netherlands; <sup>c</sup>Laboratory for Chemistry and Life Science, Institute of Innovative Research, Tokyo Institute of Technology, 226-8503 Yokohama, Japan; and <sup>d</sup>Department of Biology, Chemistry Faculty, National Autonomous University of Mexico, 04510 Mexico City, Mexico

Edited by Martin Karplus, Harvard University, Cambridge, MA, and approved October 9, 2020 (received for review February 26, 2020)

The rotation of *Paracoccus denitrificans*  $F_1$ -ATPase (PdF<sub>1</sub>) was studied using single-molecule microscopy. At all concentrations of adenosine triphosphate (ATP) or a slowly hydrolyzable ATP analog (ATP $\gamma$ S), above or below  $K_m$ , PdF<sub>1</sub> showed three dwells per turn, each separated by  $120^\circ$ . Analysis of dwell time between steps showed that PdF<sub>1</sub> executes binding, hydrolysis, and probably product release at the same dwell. The comparison of ATP binding and catalytic pauses in single PdF<sub>1</sub> molecules suggested that PdF<sub>1</sub> executes both elementary events at the same rotary position. This point was confirmed in an inhibition experiment with a nonhydrolyzable ATP analog (AMP-PNP). Rotation assays in the presence of adenosine diphosphate (ADP) or inorganic phosphate at physiological concentrations did not reveal any obvious substeps. Although the possibility of the existence of substeps remains, all of the datasets show that PdF<sub>1</sub> is principally a three-stepping motor similar to bacterial vacuolar ( $V_1$ )-ATPase from *Thermus thermophilus*. This contrasts with all other known  $F_1$ -ATPases that show six or nine dwells per turn, conducting ATP binding and hydrolysis at different dwells. Pauses by persistent Mg-ADP inhibition or the inhibitory  $\zeta$ -subunit were also found at the same angular position of the rotation dwell, supporting the simplified chemomechanical scheme of PdF<sub>1</sub>. Comprehensive analysis of rotary catalysis of  $F_1$  from different species, including PdF<sub>1</sub>, suggests a clear trend in the correlation between the numbers of rotary steps of  $F_1$  and  $F_0$  domains of F-ATP synthase.  $F_1$  motors with more distinctive steps are coupled with proton-conducting  $F_0$  rings with fewer proteolipid subunits, giving insight into the design principle the  $F_1F_0$  of ATP synthase.

$F_1$ -ATPase | rotation | single-molecule analysis |  $\zeta$ -subunit

**F**<sub>1</sub> $F_0$ -ATP synthase (or F-ATP synthase) is nature's smallest rotary motor and produces most of a cell's chemical energy in the form of adenosine triphosphate (ATP). Powered by a transmembrane electrochemical ion gradient, this enzyme catalyzes the synthesis of ATP from adenosine diphosphate (ADP) and inorganic phosphate ( $P_i$ ) (1). F-ATP synthase is composed of two rotary molecular motors, named as  $F_1$  and  $F_0$ . Water-soluble  $F_1$  catalyzes the synthesis (when complexed with  $F_0$ ) or hydrolysis of ATP, and membrane-embedded  $F_0$  conducts translocation of  $H^+$  or  $Na^+$  ions (2) across the membrane (3–5).  $F_1$  and  $F_0$  form the whole complex of F-ATP synthase, connecting together via a central and a peripheral stalk (6).

$F_1$  (also known as  $F_1$ -ATPase) remains catalytically active as an ATPase when it is isolated from  $F_0$ , and its rotary catalysis mechanism has been widely studied.  $F_1$  is composed of a hexameric catalytic core, formed by  $\alpha_3\beta_3$ -subunits, that surrounds a central rotary shaft formed by a  $\gamma/\epsilon$ -subcomplex (7, 8). Each  $\alpha/\beta$ -interface in the  $\alpha_3\beta_3$ -ring has a catalytic reaction center, while most of catalytic residues reside on the  $\beta$ -subunit. The three  $\beta$ -subunits exhibit significant differences in their affinity for

Mg<sup>2+</sup> nucleotides, adopting three functionally distinct conformations. Each conformational state of the  $\beta$ -subunit is designated as  $\beta_T$ ,  $\beta_D$ , or  $\beta_E$  (8, 9).

Single-molecule and biochemical studies have established that hydrolysis of ATP by  $F_1$  or  $F_1F_0$  produces continuous rotation of the central shaft in a counterclockwise (CCW) direction when viewed from the membrane (10). The rotation results from the repetition of discrete  $120^\circ$  cycles in which the three  $\beta$ -subunits cooperatively change their conformation and one ATP molecule is consumed (11).

Extensive single-molecule studies from the *Bacillus* strain PS3  $F_1$  (TF<sub>1</sub>) (10, 12–14) elucidated a detailed chemomechanical coupling mechanism of a bacterial enzyme (Fig. 1A) that was later supported by the description of the *Escherichia coli*  $F_1$  (EF<sub>1</sub>) (15–19). In these bacterial enzymes, each  $120^\circ$  cycle is further divided into two substeps, resulting in six intervening dwells per turn. An  $80^\circ$ – $85^\circ$  substep is triggered by ATP binding and the concurrent ADP release that occurs on two different  $\beta$ -subunits, and another  $40^\circ$ – $35^\circ$  substep is initiated after ATP cleavage and triggered by the release of  $P_i$ , which occurs

## Significance

F-ATP synthase is a fundamental enzyme supplying adenosine triphosphate (ATP), spreading across all kingdoms of life. Despite remarkable conservation of its basic structure and function, biophysical studies have revealed discrete differences in the rotary mechanisms of bacterial and eukaryotic  $F_1$ -ATPases (the catalytic portions of the enzymes). Here, we analyzed the rotational dynamics of *Paracoccus denitrificans*  $F_1$  (PdF<sub>1</sub>), a bacterial  $F_1$ -ATPase that exhibits high homology with the core functional subunits of its mitochondrial counterpart. Notably, PdF<sub>1</sub> possesses a simplified chemomechanical scheme different from that of all other  $F_1$ -ATPases. Our results reveal an unexpected diversity in the chemomechanical coupling cycle of the  $F_1$ -ATPase machinery and show that features such as homology or phylogenetic relationship cannot uniquely define the rotary scheme pattern.

Author contributions: M.Z.-Z., D.G.G.M., T.S., H.U., J.J.G.-T., and H.N. designed research; M.Z.-Z., R.W., and F.M.-H. performed research; J.J.G.-T. and H.N. contributed new reagents/analytic tools; M.Z.-Z. and R.W. analyzed data; and M.Z.-Z. wrote the paper.

The authors declare no competing interest.

This article is a PNAS Direct Submission.

This open access article is distributed under Creative Commons Attribution-NonCommercial-NoDerivatives License 4.0 (CC BY-NC-ND).

<sup>1</sup>To whom correspondence may be addressed. Email: marielzarco\_zavala@comunidad.unam.mx, jgartre@unam.mx, or hnoji@g.ecc.u-tokyo.ac.jp.

This article contains supporting information online at <https://www.pnas.org/lookup/suppl/doi:10.1073/pnas.2003163117/-DCSupplemental>.

First published November 9, 2020.

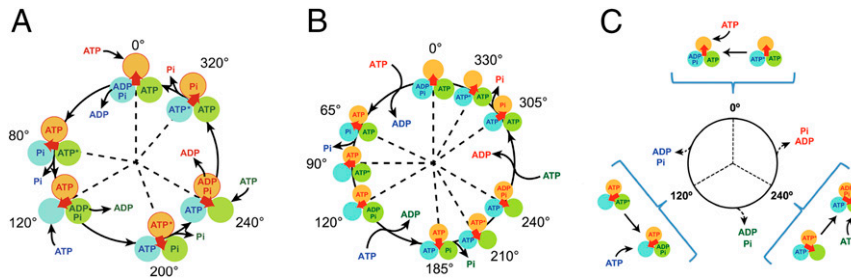


**Fig. 1.** Proposed chemomechanical coupling schemes of the (A) bacterial  $TF_1$ , (B) eukaryotic  $hMF_1$ , and (C)  $Pcf_1$ . In all images, each circle represents the chemical state of the catalytic site in each  $\beta$ -subunit, the central red arrow represents the orientation of the  $\gamma$ -subunit, ATP\* represents the prehydrolysis state of ATP, and 0° is defined as the ATP binding angle for the catalytic site at the 12 o'clock position. In C, dashed arrows indicate that the simultaneous release of  $P_i$  and ADP has not yet been precisely determined.

sequentially at two different  $\beta$ -subunits. The dwells before the 80°–85° and 40°–35° substeps are referred to as binding and catalytic dwells, respectively.

Mitochondrial  $F_1$  exhibits a variety of chemomechanical coupling schemes different from that of its bacterial counterpart (20–23). Human mitochondrial  $F_1$  ( $hMF_1$ ) (Fig. 1B) and bovine mitochondrial  $F_1$  ( $bMF_1$ ) exhibit a chemomechanical coupling scheme in which each 120° cycle is composed of three substeps, and nine intervening pauses form one revolution (20, 21). Both enzymes display two intervening dwells associated with catalytic and binding states (with an angular displacement of 90° for  $hMF_1$  and 80° for  $bMF_1$ ) in addition to a third intervening pause (located at 65° from the binding dwell in  $hMF_1$  and 10°–20° in  $bMF_1$ ). Single-molecule studies and crystallographic evidence have associated the third intervening pause in  $hMF_1$  with a pre- $P_i$  release state (21, 24). However, the identity of the catalytic state that is associated with the third dwell in the case of  $bMF_1$  remains elusive (20).

Despite its high homology, the rotation dynamics of *Saccharomyces cerevisiae*  $F_1$  ( $YMF_1$ ) (22) show several differences from other mitochondrial  $F_1$ 's. Consistent with all  $F_1$ -ATPases, this enzyme displays two clear intervening pauses associated with catalytic and binding states. However, no clear evidence of a third intervening dwell has been uncovered.

Since the minimal  $F_1$  structural morphology remains conserved among bacteria and mitochondrial enzymes, the differences between their chemomechanical mechanisms may suggest adaptation and/or additional undescribed function(s). To gain insight into the understanding of these differences, we studied the mechanical properties of the  $F_1$ -ATPase of the  $\alpha$ -proteobacterium *Paracoccus denitrificans* (Pd), a bacterial model organism used in the bioenergetic field to study eukaryotic respiratory enzymes. This organism has been proposed to have common ancestry with mitochondria (25), and its respiratory chain has many similarities with the mitochondrial one.

$PdF_1F_0$ -ATPase has a canonical bacterial composition and high amino acid conservation with the core functional subunits of its mitochondrial counterpart (26). Biochemical studies showed that this enzyme exhibits tightly regulated slow ATP hydrolysis activity and high ATP synthase activity (27–29). The inhibition of ATP hydrolysis involves an inhibitor protein known as the  $\zeta$ -subunit, which is exclusively conserved in the alphaproteobacteria class (30). The  $\zeta$ -subunit possesses a structure different from the other known bacterial and mitochondrial regulatory subunits ( $\epsilon$ -subunit and ATPase inhibitory factor 1 [IF<sub>1</sub>]) (31). Still, the sequence of its inhibitory region is weakly related to that of the mitochondrial inhibitor IF<sub>1</sub> (32). Biochemical and crystallographic evidence supports the notion that the  $\zeta$ -inhibitory mechanism resembles that of IF<sub>1</sub>, in which the  $\zeta$ -intrinsically disordered inhibitory domain adopts a helical structure after occupying its inhibitory

position in the  $\alpha_D\beta_D$ -catalytic interface of its cognate  $F_1$ , equivalent to IF<sub>1</sub> (26, 33).

Here, we analyzed the rotary dynamics of the recombinant expressed  $PdF_1$ . Unexpectedly,  $PdF_1$  rotation exhibits only three intervening pauses per revolution (separated by 120°), and no obvious substeps were resolved. ATP binding and ATP hydrolysis apparently occur at the same angular position, revealing a chemomechanical coupling mechanism unique among currently characterized  $F_1$ -ATPases (Fig. 1C). Furthermore, we directly show that Mg-ADP and the  $\zeta$ -subunit partially and totally inhibit the rotation of  $PdF_1$ , respectively. Our results suggest that both entities exert a regulatory role in determining the latent hydrolytic activity of  $PdF_1F_0$  ATP synthase.

## Results

**Recombinant Expression of  $PdF_1$ .** The protein expression of the recombinant  $PdF_1$  complex in the *E. coli* system was investigated in the presence and absence of coexpressed Atp12p, the *P. denitrificans* homolog of ATPAF2, an assembly factor of mitochondrial  $F_1$  (34). Native polyacrylamide gel electrophoresis (PAGE) of the cytoplasmic fractions of the recombinant cells showed that coexpression of Atp12p significantly enhanced the expression of the  $PdF_1$  complex (SI Appendix, Fig. S1A), revealing that the Atp12 protein is essential for the efficient production and assembly of  $PdF_1$ . This is a demonstration of this chaperone functioning in the assembly of a bacterial  $F_1$ -ATPase.

Previous studies revealed the importance of ATPAF1 (*Atp11*) and ATPAF2 (*Atp12*) in the assembly of the eukaryotic  $F_1$ , which have been proposed to prevent the aggregation of the  $\beta$ - and  $\alpha$ -subunits (35). The conservation of the *Atp12* gene in the alphaproteobacteria genome (36) and its role in the building of the *P. denitrificans* enzyme evince a high similarity in the assembly process of  $PdF_1$  and mitochondrial  $F_1$ .

To examine the rotary dynamics of the Pd enzyme, the mutant " $PdF_1 \gamma CC$ " (a  $PdF_1$ -ATPase with the following modifications:  $\beta$ His tag,  $\gamma Q115C$ , and  $\gamma D214C$ ) was engineered. Purified  $PdF_1 \gamma CC$  was biotinylated with sodium dodecyl sulfate (SDS)-PAGE and western blot analysis, revealing an appropriate subunit composition and the specific biotinylation of the  $\gamma$ -subunit (Materials and Methods and SI Appendix, Fig. S1 B and C).

**ATP Hydrolysis of  $PdF_1 \gamma CC$ .**  $PdF_1$  typically has tightly regulated ATP hydrolysis activity (27), which can be partially relieved by the removal of its intrinsic regulatory  $\zeta$ -subunit or by the presence of either lauryldimethylamine oxide (LDAO) or oxyanions (28, 32). We quantified the hydrolytic activity of  $PdF_1 \gamma CC$  in the absence of an activator. As expected, since our recombinant complex does not contain the inhibitory  $\zeta$ -subunit, an ATPase-specific activity of  $5.1 \pm 0.4 \text{ s}^{-1}$  ( $\pm$  SE; 0.85 units per milligram of protein) was observed, higher than that reported for  $PdF_1$

purified from *P. denitrificans* cells (0.14 units per milligram of protein) but similar to the activity of pure F<sub>1</sub> obtained from a *P. denitrificans*  $\zeta$ -knockout strain (Pd $\Delta\zeta$ ; 0.87 units per milligram of protein) (37). Furthermore, the addition of 0.1% LDAO resulted in an 11-fold increase in activation, showing a specific activity of  $56.7 \pm 3.6 \text{ s}^{-1}$  ( $\pm$  SE) (Fig. 2B), similar to but higher than the fivefold activation obtained with the PdF<sub>1</sub> $\Delta\zeta$  preparation when LDAO is included in the assay (37). Additionally, the reconstitution of the  $\zeta$ -subunit led to a complete inhibition of PdF<sub>1</sub>  $\gamma$ CC ATP hydrolytic activity, in agreement with previous studies (26, 32) (SI Appendix, Fig. S1D). Overall, these data corroborated the biochemical characteristics of PdF<sub>1</sub>  $\gamma$ CC, confirming that the recombinant mutant possesses similar characteristics to the native PdF<sub>1</sub>. For simplicity, PdF<sub>1</sub>  $\gamma$ CC is referred to as PdF<sub>1</sub> hereafter.

**Rotation Assay of PdF<sub>1</sub>.** PdF<sub>1</sub> was immobilized onto a nickel-nitrilotriacetic acid-coated glass via polyhistidine tags. The rotation was observed with a 40-nm gold nanoparticle attached to the  $\gamma$ -subunit as a probe (Fig. 2A). Images were taken with a high-speed camera at a recording speed of 10,000 frames per second (fps; 100  $\mu$ s per frame). However, because PdF<sub>1</sub> possesses a latent ATP hydrolysis activity, almost no rotating particles were detected. Therefore, an ATPase activator (0.1% LDAO) and an ATP regeneration system were included in the reaction buffer. Under this condition, we easily observed CCW rotation of PdF<sub>1</sub> that was frequently interrupted by periods of rotation pause (likely caused by Mg-ADP inhibition; see below).

The overall speed of rotation, calculated from the lapses in continuous rotation, followed simple Michaelis-Menten kinetics

with an apparent  $K_m$  for ATP of  $78 \pm 5 \mu\text{M}$  and  $V_{\text{max}}$  of  $338 \pm 6$  ( $\pm$  SE) revolutions per second (rps) (Fig. 2B). Using these kinetic parameters, we estimated an apparent  $k_{\text{on}}$  for ATP of  $1.3 \times 10^7 \text{ M}^{-1} \text{ s}^{-1}$ , which was comparable with the  $k_{\text{on}}$  values of  $3.0 \times 10^7$  and  $2.7 \times 10^7 \text{ M}^{-1} \text{ s}^{-1}$  for TF<sub>1</sub> and hMF<sub>1</sub>, respectively (13, 21).

Interestingly, the maximum velocity obtained from single-molecule data (338 rps) mismatches that quantified by biochemical ATPase assay (ATPase/3 = 18.9 rps) (Fig. 2B). Previous evidence has shown a similar trend in the case of some F<sub>1</sub>-ATPases, where these discrepancies have been attributed to Mg-ADP-mediated inhibition or to the selection of functional rotating enzymes in single-molecule experiments (21, 38, 39). Biochemical studies suggested that Mg-ADP regulates PdF<sub>1</sub>-ATPase activity (40). Later, we explore the direct effect of Mg-ADP on PdF<sub>1</sub> rotary catalysis.

### PdF<sub>1</sub>-ATPase Exhibits Three-Step Rotation Regardless of the Concentration of ATP.

The stepping behavior of PdF<sub>1</sub> was closely examined under low ATP concentration ( $\ll K_m$ ), middle ATP concentration (near  $K_m$ ), and high ATP concentration ( $\gg K_m$ ). Previous single-molecule rotation studies revealed that, independent of their origin, all investigated F<sub>1</sub>-ATPases display substeps in each 120° cycle (13, 15, 21, 22, 39, 41). For instance, TF<sub>1</sub>, the archetypal bacterial F<sub>1</sub>-ATPase for single-molecule studies, has two substeps, and hMF<sub>1</sub> has three substeps in each 120° cycle (Fig. 1 A and B). Since the dwell positions between steps at high and low ATP concentrations are generally different, substep behaviors are normally observed in F<sub>1</sub>-ATPases at ATP concentrations near  $K_m$ . However, PdF<sub>1</sub> does not exhibit any

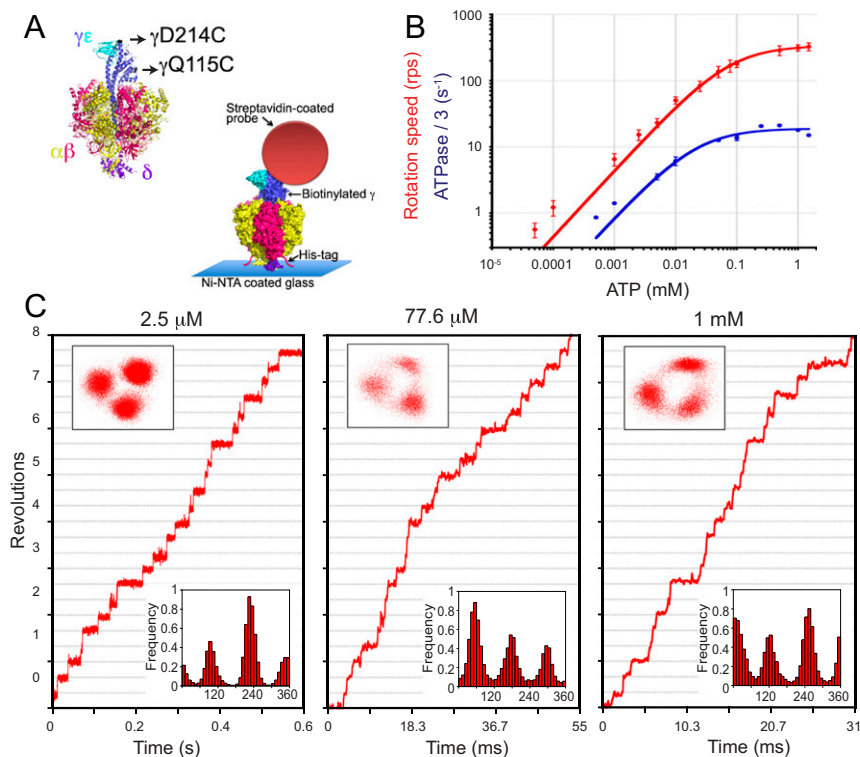


**Fig. 2.** ATP-driven rotation of PdF<sub>1</sub>. (A) Single-molecule setup of PdF<sub>1</sub>. Two cysteine residues of the rotor  $\gamma$ -subunit (black arrows) were used to attach the rotary probe using biotin-streptavidin, and His tag in the  $\beta$ -subunit was used to immobilize PdF<sub>1</sub> to the Ni-coated glass. (B) Time-averaged rotation speed of PdF<sub>1</sub> (red) and one-third of the bulk-phase ATPase rate (blue) vs. Mg-ATP concentration. Solid lines show Michaelis-Menten fits.  $V_{\text{max}} = 338 \pm 6$  rps and  $K_m = 77.6 \pm 5.3 \mu\text{M}$  for rotation and  $V_{\text{max}} = 18.9 \pm 1.2 \text{ s}^{-1}$  and  $K_m = 22.1 \pm 8.2 \mu\text{M}$  for ATPase/3. Error bars represent SD. (C) Time courses of three different rotating particles observed under different [ATP] (indicated at the top of each graph). Upper Insets and Lower Insets display  $xy$  trajectories of the centroids and angular distributions, respectively. For each particle, the reference angle was arbitrarily assigned. In B, three repetitions were done for each measurement of ATPase. In B and C, 20 rotating molecules were analyzed per condition in the single-molecule analysis. Ni-NTA, nickel-nitrilotriacetic acid.



substep, and only three intervening pauses (separated by 120°) at all [ATP] investigated were identified (Fig. 2C).

Statistical analysis of the intervals between steps under low [ATP] showed a single exponential decay function (Fig. 3A–C). The rate constants determined from the dwell time histograms ( $\tau_1$ ) were proportional to [ATP], confirming these waiting times as the ATP binding dwells (Fig. 3H). The estimated rate constant for ATP binding ( $k_{on}$ ) was  $1.6 \pm 0.3$  ( $\pm$  SD)  $\times 10^7$  M<sup>-1</sup> s<sup>-1</sup>, in agreement with the  $k_{on}$  of  $1.3 \times 10^7$  M<sup>-1</sup> s<sup>-1</sup> calculated from the Michaelis–Menten analysis.

At [ATP] near  $K_m$  (Fig. 3D) and under  $V_{max}$  conditions (Fig. 3E and F), the histograms of dwell time between successive steps obeyed a two-consecutive reaction model. Two time constants were calculated in each condition, designated as  $\tau_1'$  and  $\tau_2$  for the condition near  $K_m$  and  $\tau_2$  and  $\tau_3$  for conditions with saturated [ATP]. Time constants  $\tau_2$  and  $\tau_3$  were independent of [ATP] (Fig. 3H), supporting their association with ATP hydrolysis and product release events, while  $\tau_1'$  appears to be the sum of the binding dwell and the catalytic dwell (likely  $\tau_3$ ). Overall, these results suggest that at least three elementary reactions occur at the same angular position, most likely ATP binding ( $\tau_1$ ), ATP hydrolysis, and product release ( $\tau_2$  and  $\tau_3$ ). However, the identities of the elementary steps that correspond to  $\tau_2$  and  $\tau_3$  remain unclear.

To confirm the absence of substepping behavior in the chemicochemical coupling reaction of PdF<sub>1</sub>, we observed the rotation of PdF<sub>1</sub> in the presence of a slowly hydrolyzable ATP analog, ATP $\gamma$ S [adenosine-5'-O-(3-thiotriphosphate)], that allows a detailed analysis of the stepping rotation of F<sub>1</sub>. The slowed ATP $\gamma$ S

catalysis results from a deceleration of the hydrolytic reaction of TF<sub>1</sub> and bMF<sub>1</sub> (20, 42) and also, the release of a phosphate analog (thiophosphate) with the hMF<sub>1</sub> enzyme (21). ATP $\gamma$ S-driven rotation of PdF<sub>1</sub> obeyed a Michaelis–Menten model (SI Appendix, Fig. S2A), giving a  $K_m$  of  $1.8 \pm 0.3$   $\mu$ M and  $V_{max}$  of  $5.9 \pm 0.2$  rps ( $\pm$  SE).  $V_{max}$  was 57-fold slower than its rotation with ATP (338 rps). As with ATP, PdF<sub>1</sub> exhibited only 120° steps at all [ATP $\gamma$ S] examined (SI Appendix, Fig. S2), supporting the absence of additional subpauses.

We analyzed the duration of the pauses displayed at different ATP $\gamma$ S concentrations. We observed that at low [ATP $\gamma$ S], the histogram of dwell time obeyed a single-reaction model, and one reaction constant was estimated ( $\tau_1$ ) (SI Appendix, Fig. S3A). At concentrations near  $K_m$  and saturated [ATP $\gamma$ S], histograms of dwell time followed a double exponential function (SI Appendix, Fig. S3 B–F).

The reaction constants estimated at saturated [ATP $\gamma$ S] (designated as  $\tau_2$  and  $\tau_3$ ) were independent of the substrate concentration (SI Appendix, Fig. S3 E–G), suggesting their association with the hydrolytic event or product release. Neither were similar to the reaction constants estimated at saturated ATP. Therefore, we suggest that ATP $\gamma$ S extended both the hydrolytic event and the product release event. However, the exact identity of the elementary step(s) associated with  $\tau_2$  and  $\tau_3$  remains unclear.

As expected, two reaction constants were estimated at concentrations around  $K_m$ , designated  $\tau_1$  and “ $\tau_2 + \tau_3$ ” (SI Appendix, Fig. S3 B–D). The waiting times  $\tau_1$  were inversely proportional to [ATP $\gamma$ S], supporting the hypothesis that these are the binding

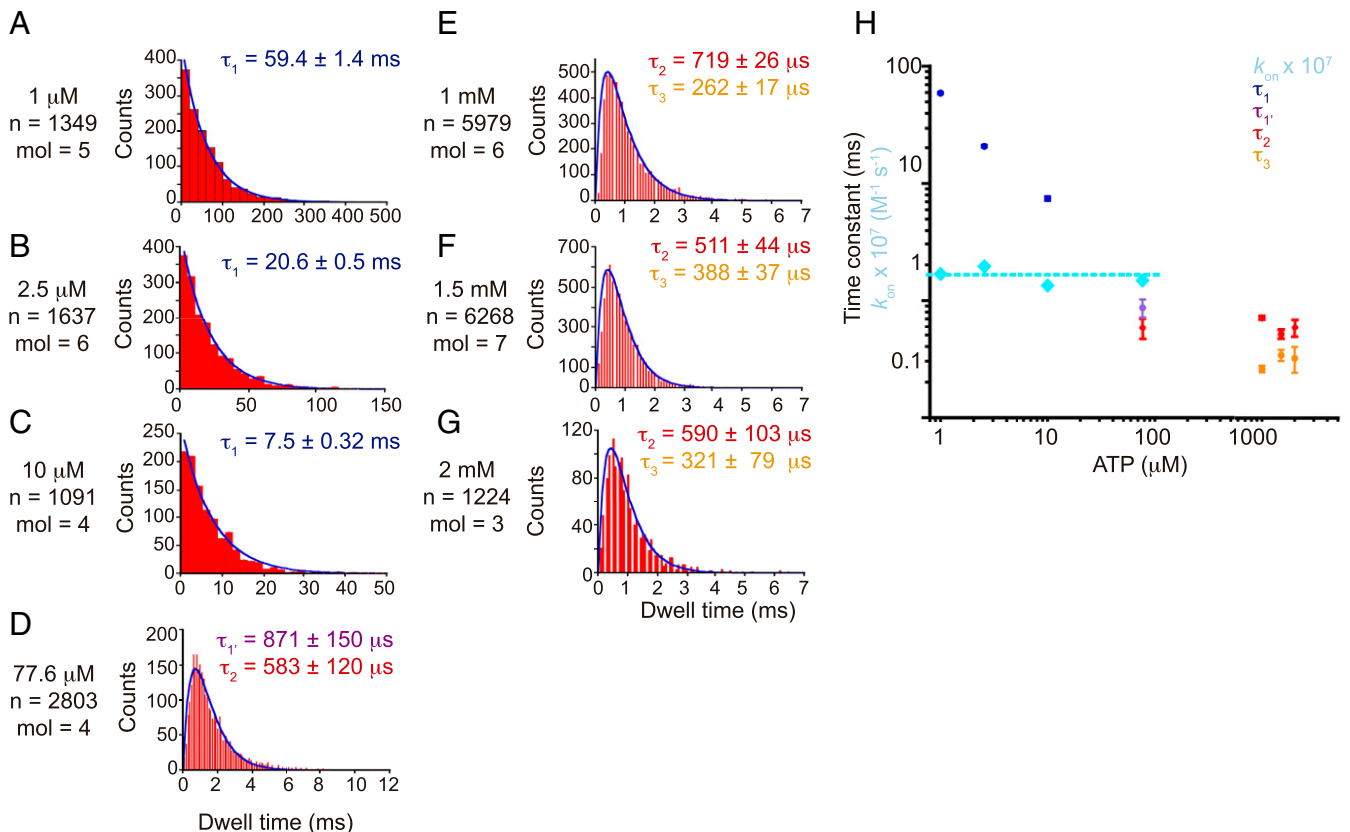


**Fig. 3.** Dwell distributions for a composite of PdF<sub>1</sub> molecules at different [ATP]. In each graph,  $\tau$  denotes the time constant calculated from fitting (solid line) a single exponential decay function (A–C) or a double exponential decay function (D–G). At the left of each graph, [ATP], the total number of dwells summed ( $n$ ), and the number of molecules collectively analyzed (mol) are displayed. (H) ATP concentration dependency of the time constants. The  $\tau_1$ -constants were used to calculate the second-order rate constant of ATP binding ( $k_{on}$ ), and the obtained values were plotted against ATP concentration in light blue squares. Error bars represent SE.

dwells (*SI Appendix, Fig. S3G*). The estimated  $k_{on}$  for ATP $\gamma$ S binding based on the values of  $\tau_1$  was  $8.2 \pm 2.6$  ( $\pm$  SD)  $\times 10^6$  M $^{-1}$  s $^{-1}$ , in agreement with the  $k_{on}$  of  $9.8 \times 10^6$  M $^{-1}$  s $^{-1}$  calculated from  $3 \times V_{max}/K_m$ , confirming that  $\tau_1$  represents the binding rate. On the other hand, the waiting times “ $\tau_2 + \tau_3$ ” were independent of the substrate concentration and appeared to be the sum of  $\tau_2 + \tau_3$  (*SI Appendix, Fig. S3G*). Overall, our results reinforce the notion that substrate binding and two other substrate-independent elementary steps occur at the primary dwells, the most likely candidates being the hydrolytic reaction and product release.

### Binding and Catalytic Dwell Share the Same Angular Position in PdF<sub>1</sub>.

The absence of any substepping behavior in the rotary mechanism of PdF<sub>1</sub> suggests that the elementary reactions may occur in the same angular position. To test this hypothesis, we compared the dwell positions of single PdF<sub>1</sub> molecules at low ATP concentration (ATP binding dwells) and those at high ATP concentration (catalytic pauses).

The increase in the rotation speed from  $14.1 \pm 2.9$  rps (at  $2.5 \mu$ M ATP) to  $343 \pm 61$  rps ( $\pm$  SD; at  $1$  mM ATP) after buffer exchange confirmed the increase in [ATP] (Fig. 4A). Examination of the bead centroid revealed three discrete  $120^\circ$  pauses under both conditions (Fig. 4B and C). The difference in dwell angles ( $\Delta\theta$ ) after increasing [ATP] was only  $0.5^\circ \pm 0.3^\circ$  ( $\pm$  SE), suggesting the catalytic pause of PdF<sub>1</sub> occurs at the same angular position of the ATP waiting pause (Fig. 4D).

For further confirmation, we identified the angular position of ATP hydrolysis using the nonhydrolyzable ATP analog 5'-adenylyl-imidodiphosphate (AMP-PNP) (43) and compared its inhibitory stall with the ATP binding events. For this, we used a 200-nm magnetic bead duplex as a probe in place of a 40-nm gold nanoparticle to give us a manipulatable “handle” on PdF<sub>1</sub>.

First, we observed the stepping rotation of a PdF<sub>1</sub> molecule under substrate-limiting conditions ( $0.5 \mu$ M ATP  $\ll K_m = 4.1 \pm 0.5 \mu$ M [ $\pm$  SE]) (*SI Appendix, Fig. S4*). Following this, a buffer containing  $0.5 \mu$ M AMP-PNP was gently introduced into the flow chamber with  $0.5 \mu$ M ATP. After the infusion of AMP-PNP, the particles continued rotating for 1 to 2 min before they stopped and did not spontaneously resume rotation through the end of the experiment (Fig. 5A). The AMP-PNP-inhibited state did not

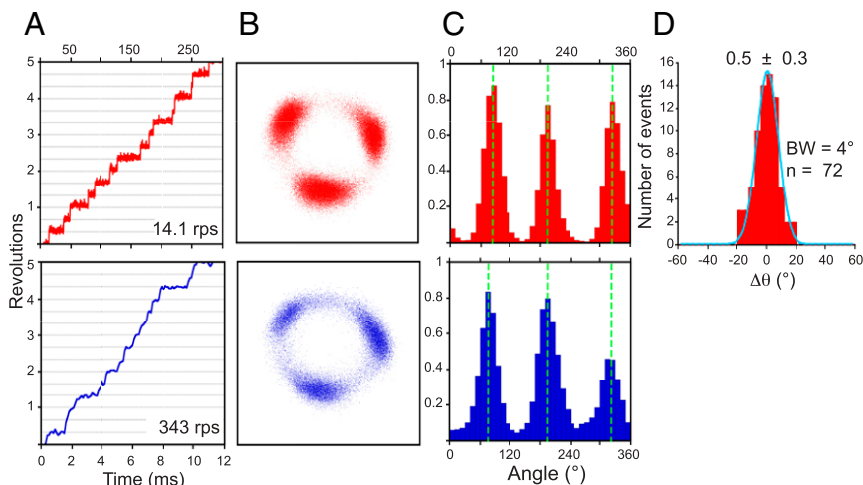


**Fig. 4.** Observation of a single rotating PdF<sub>1</sub> under low (red) and high (blue) [ATP]. One representative particle, from 24 molecules analyzed, is displayed. (A) Time courses of the rotation (rotation speed). (B) The xy position of the bead centroid. (C) Histograms of the angular position. The dashed lines highlight the mean value obtained from fitting a Gaussian distribution. (D) Distribution of the angular difference between the position of ATP cleavage relative to ATP binding ( $\Delta\theta$ ). The solid line represents the fit to a Gaussian model, and the value of the mean difference ( $\pm$  SE) is shown. For this experiment, 40-nm gold particles and a recording rate of 10,000 fps were used. BW, bin width;  $n$ , number of events analyzed.

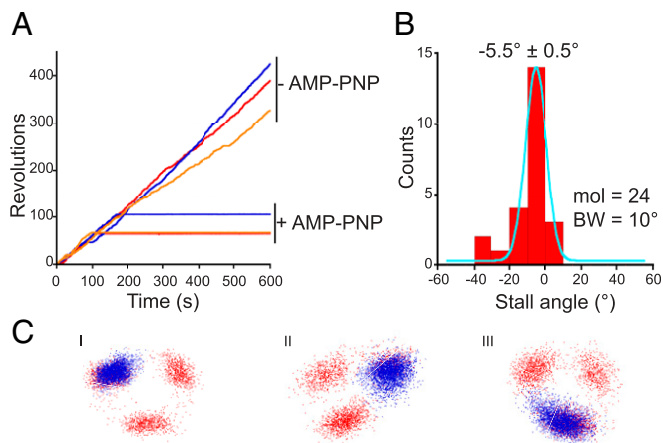


**Fig. 5.** Identification of the catalytic dwell by AMP-PNP. (A) Rotation of three PdF<sub>1</sub> molecules (red, blue, and orange) before and after the addition of  $0.5 \mu$ M AMP-PNP in the presence of  $0.5 \mu$ M ATP. A submicrometer magnetic bead was used, and recordings were taken at 60 fps at  $25^\circ$ C. (B) Angle distribution of AMP-PNP-induced stalls relative to the nearest ATP binding dwell. The solid line represents the fit to a Gaussian equation. The mean value ( $\pm$  SE) is displayed. BW, bin width; mol, molecules analyzed. (C) Stall positions of the AMP-PNP-inhibited state (blue) are superimposed on the xy trajectories (red) that show the positions of the ATP binding dwells (three representative particles are displayed).

resume active rotation even if forcibly rotated with magnetic tweezers. This allows for the discrimination of AMP-PNP inhibition from the ADP-inhibited form that is readily reactivated with magnetic tweezers (44). The angular distance ( $\Delta\theta$ ) of the AMP-PNP inhibitory state from the nearest binding angle revealed a mean difference of  $-5.5 \pm 0.5^\circ$  ( $\pm$  SE) (Fig. 5B and C), supporting the finding that the ATP binding and ATP cleavage dwells share nearly the same angular position.

Overall, these results suggest that the rotary behavior of PdF<sub>1</sub> is different from other F<sub>1</sub>'s. However, 0.1% LDAO was added to the reaction buffer in all experiments as an ATPase activator (45–47). Although single-molecule studies on other F<sub>1</sub>'s show that LDAO extends the duration of the actively rotating state and shortens the duration of the inhibitory pausing state without

affecting the principle rotation mechanism (38, 39), we analyzed the rotation of single particles in the presence and absence of the detergent (under low and saturated ATP concentrations) for confirmation that the PdF<sub>1</sub> rotary mechanism is not affected by LDAO (*SI Appendix, Fig. S5*). At both ATP concentrations, we observed that LDAO reduces both the rotation velocity of PdF<sub>1</sub> and the duration of the inactive state (likely the ADP-inhibited state) (*SI Appendix, Fig. S5 A and D*). We believe the sum of both effects resulted in the activation observed in bulk assays of PdF<sub>1</sub> (where an ensemble of molecules is analyzed). Most importantly, we compared the angular position of the ATP binding (at low ATP concentration) and hydrolytic dwells (at saturated ATP) in the presence and absence of LDAO. The angular distance ( $\Delta\theta$ ) before and after including 0.1% LDAO was only  $-5.7^\circ \pm 0.4^\circ$  ( $\pm$  SE) for limiting [ATP] (*SI Appendix, Fig. S5 B and C*) and  $-2.0^\circ \pm 0.4^\circ$  ( $\pm$  SE) for high [ATP] (*SI Appendix, Fig. S5 E and F*), confirming that LDAO did not alter the angular position of the elementary dwells and suggesting that our results are consistent with the rotary mechanism in the absence of activators.

**P<sub>i</sub> Release.** Our experimental results indicated that in the rotary mechanism of PdF<sub>1</sub>, binding and catalytic events occurred at the main dwells. The absence of any additional pauses in the PdF<sub>1</sub> rotation (aside from the primary dwells) and the estimation of three time constants in the main pauses (derived from the dwell time analysis) suggested that ADP/P<sub>i</sub> release events also occur at the same angular position. We analyzed the effect of a large amount of P<sub>i</sub> on PdF<sub>1</sub> rotation to identify the angular position of the product release events.

Previous studies revealed that the addition of high P<sub>i</sub> concentrations decelerates TF<sub>1</sub> rotation rate as a consequence of extension of the dwell associated with waiting for P<sub>i</sub> release (14). As observed in *SI Appendix, Fig. S6*, the speed of PdF<sub>1</sub> rotation, driven by 1 mM ATP, decreased as [P<sub>i</sub>] increased, leading to a ~95% decrease in velocity at 300 mM P<sub>i</sub> (*SI Appendix, Fig. S6A*). However, PdF<sub>1</sub> still showed three-stepping rotation without obvious substeps. Backward steps were also not observed at any [P<sub>i</sub>] tested (*SI Appendix, Fig. S6B*). These results suggest that PdF<sub>1</sub> is a principally three-stepping motor. However, it should be noted that the suppression effect of P<sub>i</sub> is not only by product inhibition but also, by high ionic strength, considering that 500 mM KCl or 200 mM K<sub>2</sub>SO<sub>4</sub> with comparable ionic strength to that of 300 mM P<sub>i</sub> also suppressed the rotation velocity at similar levels (*SI Appendix, Fig. S6C*).

**PdF<sub>1</sub> Torque Is Similar to That Estimated for TF<sub>1</sub>.** Previously, McMillan et al. (39) suggested that a high torque may be a characteristic of unidirectional F<sub>1</sub>F<sub>o</sub> ATP synthases, as single-molecule studies of *Caldalkalibacillus thermarum* strain TA2.A1 F<sub>1</sub>-ATPase (TA2F<sub>1</sub>) revealed. To examine whether PdF<sub>1</sub> shares this characteristic, we determined its torque using a 200-nm magnetic bead duplex as a probe and analyzed the fluctuating behavior of its rotational angle ( $\theta$ ) by employing fluctuation theorem (FT) analysis. FT analysis has been widely used to estimate the driving power of motor proteins based on fluctuations in their motion without the need for an accurate measurement of a frictional drag coefficient or the application of external stall torque (48). FT analysis of 15 PdF<sub>1</sub> rotation traces under saturating ATP (2 mM) revealed a rotary torque of  $33.8 \pm 5.4$  piconewton nanometers (pNnm), similar to the torque generated by TF<sub>1</sub> under the same experimental conditions ( $34 \pm 5.4$  pNnm) (*SI Appendix, Fig. S7*) and to the torque previously reported for TF<sub>1</sub> ( $35 \pm 2.8$  pNnm;  $\pm$  SD) (48). This analysis suggests that torque may only be an influence in totally unidirectional F<sub>1</sub> such as TA2F<sub>1</sub> (49) and that motors with latent ATP hydrolysis, such

as PdF<sub>1</sub>, are not as influenced in this way, suggesting that there is another reason for minimal ATP hydrolysis.

**Pause and Stall of PdF<sub>1</sub> Rotation by Inhibitors.** The mechanisms involved in the tight inhibition of PdF<sub>1</sub> hydrolytic activity have been intensely studied. Two primary regulatory mechanisms have been proposed: Mg-ADP inhibition (40) and  $\zeta$ -inhibition (30, 32). To determine whether the Mg-ADP inhibitory mechanism is conserved in the Pd enzyme, we observed the rotation of PdF<sub>1</sub> in the presence of 1  $\mu$ M ADP and 1  $\mu$ M ATP and the absence of an ADP-trapping system (*Fig. 6A*). Under these conditions, the continuous rotation of PdF<sub>1</sub> was frequently interrupted for pauses too long to be attributed to the ATP waiting dwell ( $240 \pm 12$  ms;  $\pm$  SE) (*Fig. 6B*). Rotation spontaneously restarted after  $21.3 \pm 0.5$  s ( $\pm$  SE) (*Fig. 6C*). The removal of free ADP by infusion of a buffer containing an ADP-trapping system into the flow chamber decreased the length and frequency of the long pauses ( $11.8 \pm 0.9$  s;  $\pm$  SE) (*Fig. 6 A and C*), supporting the conclusion that they are a result of Mg-ADP inhibition.

Next, we investigated the effect of the  $\zeta$ -subunit on PdF<sub>1</sub> rotation. We compared the rotation of single particles under limiting ATP concentration (0.5  $\mu$ M) before and after the addition of 5  $\mu$ M *P. denitrificans*  $\zeta$ -subunit (Pd $\zeta$ ) (*Fig. 6E*). The addition of Pd $\zeta$  stalled the rotation of PdF<sub>1</sub>, likely forming a stable  $\zeta$ -inhibited state from which the enzyme did not spontaneously escape within the 10-min observation period.

We also examined whether PdF<sub>1</sub> molecules in Mg-ADP inhibition or  $\zeta$ -inhibition can be reactivated with forcible rotation in the CCW direction using magnetic tweezers, as reported for ADP-inhibited TF<sub>1</sub> (44). Pausing PdF<sub>1</sub> was rotated for two revolutions in the CCW direction at 1 rps and released from the magnetic tweezers. In the case of ADP-inhibited PdF<sub>1</sub>, most of molecules resumed rotation (83.3%;  $n = 12$ ). In contrast, none of the  $\zeta$ -inhibited molecules observed resumed rotation ( $n = 13$ ), revealing an intrinsic difference in the stability and mechanism of both forms of hydrolytic inhibition.

Overall, our results confirmed that the Mg-ADP inhibitory mechanism is conserved in PdF<sub>1</sub> and revealed that the regulatory mechanism of the  $\zeta$ -subunit on PdF<sub>1</sub> is similar to the one exerted by IF<sub>1</sub> on hMF<sub>1</sub> (21). In addition, we determined the angular position of the Mg-ADP and  $\zeta$ -inhibitory states relative to the location of the ATP binding state. The statistical analysis revealed that both inhibitors stop the rotation at an angular position identical to that of the ATP waiting state (*Fig. 6 D and F*). Previous studies reported that Mg-ADP stops the rotation of the bacterial TF<sub>1</sub> enzyme at the catalytic dwell (38), similar to the effect of Mg-ADP and IF<sub>1</sub> on the rotation of the eukaryotic hMF<sub>1</sub> (21). Collectively, these data suggest that Mg-ADP and the  $\zeta$ -subunit lock the PdF<sub>1</sub> enzyme in the precatalytic step. The small angular difference between the inhibitory states and the ATP binding dwell indicates that the binding and catalytic dwells share the same angular position in PdF<sub>1</sub>.

## Discussion

We characterized the stepping rotation of *P. denitrificans* F<sub>1</sub>-ATPase. The PdF<sub>1</sub> rotates  $\gamma$ -subunit unidirectionally in a CCW direction, exhibiting only three main pauses separated by 120° at all ATP and ATP $\gamma$ S concentrations tested, above or below  $K_m$ . Three different time constants in the main pauses were obtained from analysis of dwell times, suggesting that at least two reactions other than ATP binding limit the primary dwell (likely ATP cleavage and ADP/P<sub>i</sub> release). Furthermore, no substeps were detected in PdF<sub>1</sub> under all of the conditions tested, in contrast to all other investigated F<sub>1</sub>'s that show substepping behaviors when their rotation is characterized by single-molecule studies (13, 15, 21–23, 39, 41).



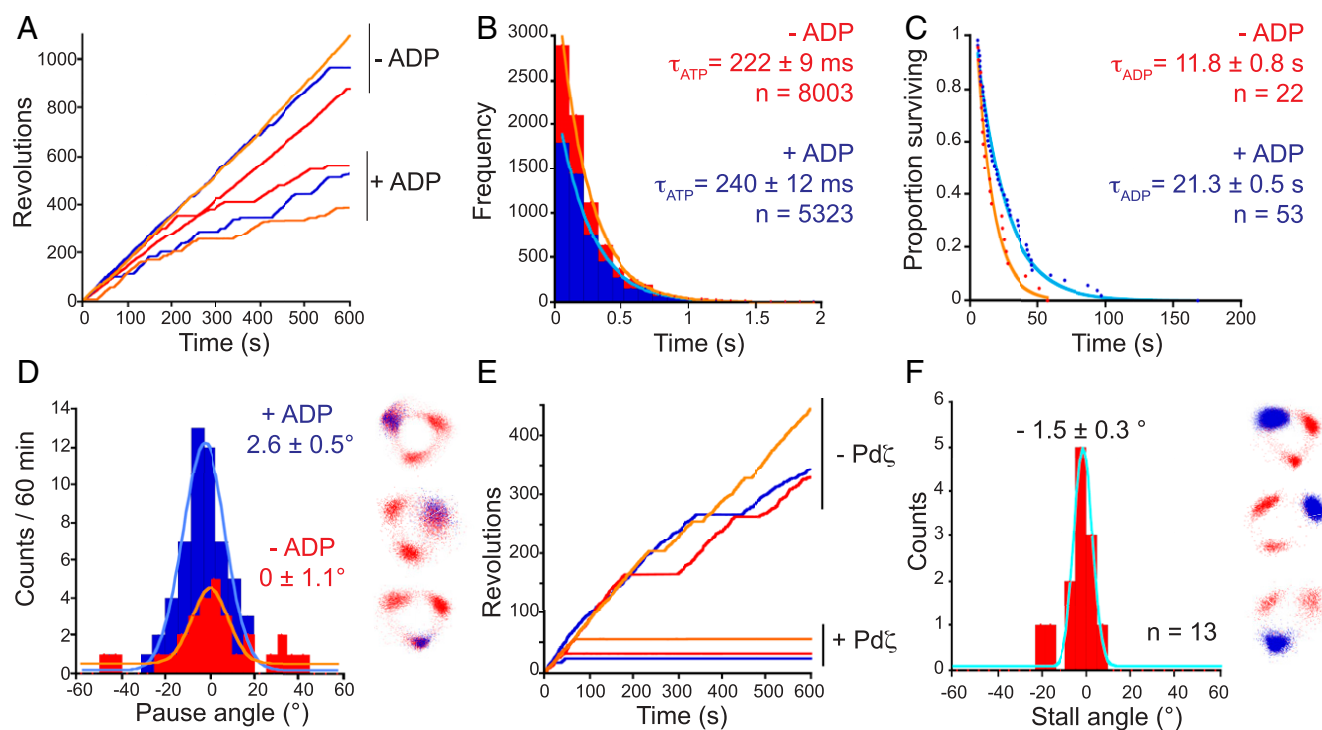


**Fig. 6.** PdF<sub>1</sub> inhibitory states. PdF<sub>1</sub> rotation was observed in the presence of limiting [ATP] and the components indicated below. (A) Rotation of three particles (red, blue, and orange) in the presence or absence of 1 μM ADP. Ten molecules were analyzed in total. (B) Dwell time analysis of the ATP binding process. Dwells shorter than 5 s were collected and collectively analyzed. (C) Decay in the number of pausing F<sub>1</sub>-ATPases in the presence (blue) or absence (red) of ADP. (D) Pausing position of the Mg-ADP-inhibited state. (E) Rotation of three particles (red, blue, and orange) before and after the addition of 5 μM Pdζ. (F) Stalling position induced by Pdζ. In B and C, solid lines show fits to single exponential functions, and time constants (± SE) are indicated. D, Left and F, Left display the angle distributions of the inhibitory states relative to the nearest ATP binding dwell. Solid lines represent fits to a Gaussian model, and the mean angular position (± SE) is indicated. In D, Right and F, Right, inhibitory states (blue) are superimposed on the xy trajectories (red) that show the ATP binding pauses (three particles are displayed). n, number of events analyzed.

The identification of ATP binding and ATP-hydrolytic dwells in single molecules revealed that both elementary steps occur at almost the same angular position in PdF<sub>1</sub>-ATPase. This result was consistent with the inhibition experiments with AMP-PNP, Mg-ADP, and the ζ-subunit, which halted PdF<sub>1</sub> rotation at  $-5.5^\circ$ ,  $2.6^\circ$ , and  $-1.5^\circ$  from the binding dwell, respectively. To date, most F<sub>1</sub>'s characterized using single-molecule techniques have shown that AMP-PNP inhibition and Mg-ADP inhibition stop rotation at the catalytic angle (21, 38), similar to the inhibitory stall of IF<sub>1</sub> on the rotation of hMF<sub>1</sub> (21), supporting the case for the absence of additional substeps in PdF<sub>1</sub> chemomechanical coupling.

Our present results suggest that at least one event in addition to ATP binding and ATP hydrolysis occurs at the position of the main dwell in PdF<sub>1</sub>, likely phosphate or ADP release (or both combined). Nevertheless, the exact ADP/P<sub>i</sub> release position in PdF<sub>1</sub> has not been directly identified. Previous studies have determined that the bacterial TF<sub>1</sub> conducts P<sub>i</sub> release at the same angular position of the catalytic dwell (14); meanwhile, the eukaryotic enzyme hMF<sub>1</sub> performs P<sub>i</sub> release at a new dwell at  $+65^\circ$  after the binding dwell (21). In the bacterial TF<sub>1</sub>, ADP release has been established at the position of the ATP binding dwell (14). An interesting finding in EF<sub>1</sub> observed that elevated [ADP] slows its rotation at  $-30^\circ$  before the catalytic dwell (23), suggesting that it has a different ADP release position than TF<sub>1</sub>.

Here, we observed that the addition of elevated concentrations of P<sub>i</sub> (SI Appendix, Fig. S6) or ADP (SI Appendix, Fig. S8) to PdF<sub>1</sub> did not expose any new dwell during its ATP-driven rotation. Neither did it extend the duration of a particular dwell in a specific manner. Therefore, the exact P<sub>i</sub> release and ADP release position in PdF<sub>1</sub> requires further investigation. These results suggest that the affinity of P<sub>i</sub> and ADP for the catalytic site after ATP

hydrolysis is low. However, in the case of ADP, we observed a dramatic reduction in the number of rotary molecules (likely caused by their arrest during the ADP inhibitory state), suggesting that ADP binding at the inhibitory position is more favorable.

Based on our results, we propose a reaction scheme for PdF<sub>1</sub> (Fig. 1C) that is strikingly similar to the rotary binding change mechanism proposed by Boyer (50), Mitchell (51), and Duncan et al. (52) and later modified by Weber and Senior (53) and Adachi et al. (14) to amend the occupancy of the catalytic sites to alternate between two and three sites. In our model, three intervening dwells compose one revolution. Any given dwell comprises ATP binding dwell, catalytic dwell, and likely product (or products) release dwell. However, the chronological order of product dissociation has not yet been directly resolved (indicated with dashed arrows in Fig. 1C). A list of possible models, although not exhaustive, is displayed (SI Appendix, Fig. S9).

It is important to emphasize that although all our experimental results show the absence of any apparent substepping behaviors in PdF<sub>1</sub> rotation and imply that all catalytic events in PdF<sub>1</sub> occur at the primary dwell position, further experiments are necessary to establish the exact position of product release. Nevertheless, the coincidence of angles for ATP binding and catalysis is distinctive from what is observed in all other characterized F<sub>1</sub>-ATPases. Furthermore, under all of the conditions presented here, there is no evidence of new subpauses associated with the ADP/P<sub>i</sub> release dwell. It is safe to conclude that the PdF<sub>1</sub> chemomechanical scheme is different from the schemes of all other known bacterial or eukaryotic F<sub>1</sub>-ATPases.

The exact elementary steps that trigger PdF<sub>1</sub> γ-rotation remain elusive. However, we suggest ATP binding as the primary

**Table 1. Stepping pattern of PdF<sub>1</sub>F<sub>o</sub> and other rotary ATPases**

Protein	Protein thermostability	Domain of life	Physiological function	Proteolipid/ring	Dwell/turn in F <sub>1</sub> /V <sub>1</sub>	Source
TF <sub>1</sub> F <sub>o</sub>	Thermophile	Bacteria	ATP synthase/hydrolase	10*	6 <sup>†,‡</sup>	(13, 66)
EF <sub>1</sub> F <sub>o</sub>	Mesophile	Bacteria	ATP synthase/hydrolase	10*	6 <sup>†,§</sup>	(15, 67)
hMF <sub>1</sub> F <sub>o</sub>	Mesophile	Eukarya	ATP synthase	8 <sup>¶</sup>	9 <sup>†,‡</sup>	(21, 65)
bMF <sub>1</sub> F <sub>o</sub>	Mesophile	Eukarya	ATP synthase	8 <sup>#</sup>	9 <sup>†,‡</sup>	(20, 65)
YMF <sub>1</sub> F <sub>o</sub>	Mesophile	Eukarya	ATP synthase	10 <sup>#</sup>	6 <sup>†,§</sup>	(6, 22)
PdF <sub>1</sub> F <sub>o</sub>	Mesophile	Bacteria	ATP synthase	12 <sup>#</sup>	3 <sup>†,‡</sup>	(33); this study
TtV <sub>1</sub> V <sub>o</sub> **	Thermophile	Bacteria	ATP synthase	12*	3 <sup>†,‡</sup>	(62, 68)
EhV <sub>1</sub> V <sub>o</sub> **††	Mesophile	Bacteria	ATP hydrolase	10 <sup>#</sup>	6 <sup>†,‡</sup>	(63, 69)

\*Values confirmed by electron cryomicroscopy analysis.

†Values determined by single-molecule analysis using gold nanoparticles as a rotary probe.

‡Forty-nanometer gold nanoparticles were used.

§Sixty-nanometer gold nanoparticles were used.

¶Values suggested according to phylogenetic analysis.

#Values confirmed by crystallography.

\*\*Tt (*Thermus thermophilus*).

††Eh (*Enterococcus hirae*).

torque-generating step, consistent with the rotary mechanism of other F<sub>1</sub>-ATPases (23, 54–56), although there remains the possibility that another reaction step is responsible for torque generation. Due to the unique rotary scheme of PdF<sub>1</sub>, the exact position and order of product releasing steps remain uncertain in this enzyme. Currently, the only resolved crystallographic structure of PdF<sub>1</sub> is in the ζ-inhibitory state (Protein Data Bank ID code 5DN6) (33), in which the rotation is likely hindered in the catalytic dwell. In this structure, one catalytic site is empty, and the remaining catalytic sites hold Mg-ATP. If we assume that this crystal structure represents a catalytic intermediate state, the nucleotide occupancy of this crystal would suggest that the release of the products from the previous intermediate state with full occupation (one catalytic site occupied by one or both products and the remaining sites holding Mg-ATP) occurs before the hydrolysis of ATP (*SI Appendix, Fig. S9*). However, other

models should not be rejected. High-resolution structural analysis and further stall and release experiments could elucidate the fine details of the chemomechanical scheme of PdF<sub>1</sub>.

Two main differences between the rotary scheme of PdF<sub>1</sub> and other F<sub>1</sub>'s were observed: 1) the angular difference between the binding and catalytic dwells and 2) the total number of dwells per revolution. To date, all characterized F<sub>1</sub>'s conduct ATP binding and ATP cleavage in two different dwells (at 80° to 90° apart from each other) and display six (TF<sub>1</sub>, EF<sub>1</sub>, and YMF<sub>1</sub>) (13, 15, 22) or nine (bMF<sub>1</sub> and hMF<sub>1</sub>) (20, 21) pauses per turn, depending on the presence of an additional dwell, likely associated with P<sub>i</sub> release (21). Although it is interesting to note that advanced statistical analysis suggests that TF<sub>1</sub> makes small substeps during catalytic dwell, this has not been resolved experimentally or by conventional analysis methods (57). On the other hand, PdF<sub>1</sub> conducts ATP cleavage and ATP binding almost at the same dwell, and only three intervening pauses per turn could be identified.

We tentatively propose that variations in the F<sub>1</sub> rotary schemes could be attributable to discrete differences between their overall structures. The γ-subunit is the most plausible candidate for this structural diversity, given that Pd-γ has lower amino acid conservation than Pd-α and Pd-β compared with their mitochondrial and bacterial counterparts (*SI Appendix, Table S1*). Coincidentally, in silico modeling showed that the alteration of specific portions of the γ-subunit could affect the energetic barriers that define the stepped rotary pattern of the bMF<sub>1</sub> enzyme (58).

Interestingly, a similar rotary scheme, where ATP cleavage and ATP binding occur at nearly the same angle, has been observed in various vacuolar ATPases (V<sub>1</sub>-ATPases) and archaeal ATPases (A<sub>1</sub>-ATPases) (59–61), a group of molecular motors distantly related to F<sub>1</sub>-ATPase that conserve a similar holostucture and rotary mechanism. Analogous to the F<sub>1</sub>-ATPases, V<sub>1</sub>- and A<sub>1</sub>-ATPases exhibit a variety of stepping behaviors, and rotary schemes with three (62) and six pauses/turn (63) have been identified. Previous studies have tried to discern the features of the ATPase machinery that could determine the stepping behavior of their rotary schemes. However, results indicate that characteristics such as thermostability, phylogenetic domain, or physiological function could not uniquely define the pattern of catalytic dwell angles (Table 1).

Here, we observed an inverse correlation between the number of steps in the rotary scheme of F<sub>1</sub>/V<sub>1</sub> and the number of proteolipids per oligomer ring in their respective ion-conducting motors (F<sub>o</sub>/V<sub>o</sub>) (Fig. 7) (64). Thus, we propose that this feature could be related to the evolutionary adaptation of the chemomechanical coupling. Structural studies have suggested different copy

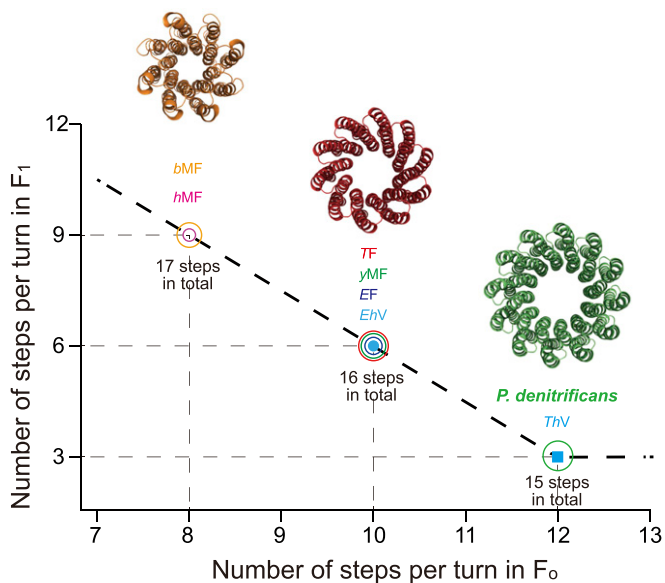


**Fig. 7.** Comparison of number of proteolipid subunits per ring vs. the number of steps/turn in the rotary scheme of F<sub>1</sub>- and V<sub>1</sub>-ATPases. Shown is a comparison of TF (*Bacillus PS3*), EF (*E. coli*), hMF (human mitochondria), bMF (bovine mitochondria), YMF (*S. cerevisiae*), PdF (*P. denitrificans*), TtV (*Thermus thermophilus*), and EhV (*Enterococcus hirae*). Structures of the c8 ring of bMF<sub>o</sub> (orange), c10 ring of TF<sub>o</sub> (red), and c12 ring of PdF<sub>o</sub> (lime green) are shown. Details and appropriate references are in Table 1.



numbers of proteolipids ( $n$ ) in the  $F_0/V_0$  ring, depending on the organism they come from (6, 33, 65–69). The “ $n$ ” value matches the number of ions transported per turn of the  $F_0/V_0$  ring (when each proteolipid possesses one binding site for one coupling ion) and has been related to the stepping pattern of the rotary ring (4, 62).

Notably, in all of the enzymes we analyzed, ATPases with more steps co-occur with ion-conducting motors with fewer steps, resulting in a total number of steps that varies from 15 to 17 (Fig. 7). We believe these values could be related to the designed potential minima that govern the ATPase machinery. This could derive from symmetry or asymmetry between  $n$  and the three catalytic subunits in  $F_1/V_1$ . However, due to limited information, only F/V ATP synthases with ring stoichiometries of 8, 10, or 12 were analyzed. It would be interesting to investigate the stepping behavior of ATPases coupled with  $F_0/V_0$  rings with different numbers of proteolipids (70–73), considering that a minimum of three steps in the  $F_1/V_1$  portion should be maintained according to total conservation of the threefold symmetry of this portion. Further studies will elucidate whether this correlation reflects a selection pressure that determines the stepping action of  $F_1$ - and  $V_1$ -ATPases and if this trend could reveal a common design principle of the rotary ATPase family.

Finally, we explored the features that define the latency of the  $PdF_1F_0$  complex in the hydrolysis of ATP. A previous study suggested that the differences in torque across species may be related to their resistance to rotation in the hydrolytic direction (39). The torque of  $PdF_1$  (33.8 pNm) did not fully reflect the lack of ATP hydrolysis that characterized the  $PdF_1$  complex and is very similar to the one estimated for hydrolytically active  $TF_1$  (34 pNm). This result suggests that, at least in the case of  $PdF_1$ , the overall structure determines the basic properties of its rotary dynamics, with the main influence on physiological function derived from regulatory mechanisms.

Currently, there is an ongoing discussion to determine if the  $\zeta$ -subunit or Mg-ADP has the dominant influence in the latent hydrolysis of  $PdF_1F_0$ . Recently, two *P. denitrificans* mutants lacking the  $\zeta$ -subunit gene were studied. One  $\zeta$ -knockout causes a specific growth defect associated with the activation of the ATP hydrolytic activity of  $PdF_1F_0$  (37). However, the other knockout caused only a moderate increase in  $PdF_1F_0$  ATP hydrolysis, which is insufficient to activate the membrane ATPase (74). We have previously hypothesized which differences in the strains could explain these apparent discrepancies (75).

In this study, we confirmed that Mg-ADP and the  $\zeta$ -subunit tightly regulate  $PdF_1$ -ATPase activity. However, we observed stark differences in the mean lifetime of their inhibitory states and their tendency to reactivate ATP hydrolysis from an inactive state. While Mg-ADP inhibition has a mean duration of  $\sim 30$  s and its inhibitory action is spontaneously relieved, the  $\zeta$ -subunit-mediated inhibition period is extended for more than 500 s and is not spontaneously relieved. These differences suggest that Mg-ADP only modulates  $PdF_1$ -ATPase activity, whereas the  $\zeta$ -subunit completely blocks the rotation of the enzyme in the hydrolytic direction. Overall, our results support the  $\zeta$ -subunit acting as a total inhibitor of  $PdF_1$  ATP hydrolysis (in vitro) and are in accordance with a critical role of  $\zeta$  as a physiological  $PdF_1F_0$ -ATPase inhibitor as described by Mendoza-Hoffmann et al. (37).

In summary, our results indicate that the reaction scheme of  $PdF_1$  is likely different from that of other bacterial and eukaryotic  $F_1$ -ATPases, despite its high conservation with its mitochondrial

counterpart. This finding suggests that subtle differences (in the structure or sequence) can heavily influence the rotary mechanism of  $F_1$ . Additionally, substepping behaviors are not a prerequisite for successful rotation and torque production in  $F_1$ -ATPase. Whether the simplified rotary mechanism of  $PdF_1$  is conserved in other  $F_1$ 's of the alphaproteobacteria class remains unknown. However, since substantial evidence supports alphaproteobacteria being closely related to the proto-endosymbiont from which mitochondria emerged (25), we believe that future comparative and phylogenetic analyses could provide interesting information regarding the evolution of the mitochondrial  $F_1$  rotary mechanism. How individual species deal with different rotary schemes and the advantage any of these may confer now require further study.

## Materials and Methods

**Preparation of  $PdF_1$ .** The  $F_1$  operon (atpHAGDC) and the gene of the chaperone *Atp12p* were amplified from *P. denitrificans* genomic DNA. The genes for  $\alpha$ -,  $\gamma$ -,  $\beta$ -,  $\delta$ -, and  $\epsilon$ -subunits (with a 10-histidine tag at the N terminus of the  $\beta$ -subunit) were introduced into the expression plasmid pTR19v43 to generate the plasmid “pPdF<sub>1</sub> WT.” The *atp12* gene was introduced at the end of the  $PdF_1$  operon to generate the plasmid “pPdF<sub>1</sub> WT (+ *atp12*).” In addition, Q115 and D214 residues of the  $\gamma$ -subunit were substituted to cysteine using a site-directed mutagenesis method, generating the plasmid “pPdF<sub>1</sub> $\gamma$ CC (+ *atp12*).” All of the resulting plasmids were individually transformed into an  $F_1F_0$ -deficient *E. coli* strain, DK8 (76). Finally, all of the mutant preparations were confirmed by DNA sequencing.

**Protein Purification.**  $PdF_1$  was expressed and purified as described previously (21, 39), with some minor modifications (procedure is described in detail in *SI Appendix*). The purification was performed at room temperature, and the purified  $F_1$  was stored at  $-80^\circ\text{C}$  until further use.

**Single-Molecule Rotation Assays.** The  $PdF_1$  rotation assay was performed as described previously using either a  $\sim 0.2\text{-}\mu\text{m}$  magnetic bead duplex or a 40-nm gold nanoparticle (44, 48, 77). The detailed procedures are described in *SI Appendix*.

**Torque Measurements.** The continuous torque (newtons) of  $PdF_1$  and  $TF_1$  was estimated from the rotation trajectories at 2 mM ATP using magnetic duplex beads, based on FT analysis (48). It was calculated using the equation  $n = (k_B T / \Delta\theta) \cdot \ln[P(\Delta\theta/P(-\Delta\theta))]$ , where  $k_B T$  denotes the thermal energy and  $P(\Delta\theta)$  denotes the probability density of the distance traveled within a given time. Only enzymes exhibiting clear continuous rotation and angular velocity (nearly constant for at least 5 s) were selected for the analysis. The torque of each molecule was defined as the maximum value obtained via the FT analysis when employing a 5-s moving window, with windows starting at 1-ms intervals.

**Other Procedures.** The  $Pd\zeta$ -subunit was purified as described previously (30).  $PdF_1$ -ATPase activity was monitored by enzyme-coupled pyruvate kinase/lactate dehydrogenase ATPase assays as described elsewhere.

**Data Availability.** All data are available in the text or *SI Appendix*.

**ACKNOWLEDGMENTS.** We thank Dr. R. Watanabe for critical discussion, Dr. Y. Minagawa for his help with the data acquisition software, and all members of the laboratory of H.N. for valuable comments. This work was supported in part by National Council of Science and Technology of Mexico Fund 10010 Fellowship 277592 (to M.Z.-Z.), by National Autonomous University of Mexico Grants IN-221216 (to J.J.G.-T.) and IN-217520 (to J.J.G.-T.) from the General Direction of Academic Affairs—program for the support of research and technological innovation projects, and by Japan Society for the Promotion of Science Grant 17H06355 (to H.N.).

1. P. Mitchell, Coupling of phosphorylation to electron and hydrogen transfer by a chemi-osmotic type of mechanism. *Nature* **191**, 144–148 (1961).
2. V. Leone, D. Pogoryelov, T. Meier, J. D. Faraldo-Gómez, On the principle of ion selectivity in  $\text{Na}^+/\text{H}^+$ -coupled membrane proteins: Experimental and theoretical studies of an ATP synthase rotor. *Proc. Natl. Acad. Sci. U.S.A.* **112**, E1057–E1066 (2015).
3. D. Pogoryelov et al., Microscopic rotary mechanism of ion translocation in the  $F_0$  complex of ATP synthases. *Nat. Chem. Biol.* **6**, 891–899 (2010).

4. M. G. Düser et al., 36 degrees step size of proton-driven c-ring rotation in  $F_0F_1$ -ATP synthase. *EMBO J.* **28**, 2689–2696 (2009).
5. D. G. McMillan et al.,  $A_1A_0$ -ATP synthase of *Methanobrevibacter ruminantium* couples sodium ions for ATP synthesis under physiological conditions. *J. Biol. Chem.* **286**, 39882–39892 (2011).
6. D. Stock, A. G. Leslie, J. E. Walker, Molecular architecture of the rotary motor in ATP synthase. *Science* **286**, 1700–1705 (1999).

7. E. P. Gogol, E. Johnston, R. Aggeler, R. A. Capaldi, Ligand-dependent structural variations in *Escherichia coli* F<sub>1</sub> ATPase revealed by cryoelectron microscopy. *Proc. Natl. Acad. Sci. U.S.A.* **87**, 9585–9589 (1990).
8. J. P. Abrahams, A. G. Leslie, R. Lutter, J. E. Walker, Structure at 2.8 Å resolution of F<sub>1</sub>-ATPase from bovine heart mitochondria. *Nature* **370**, 621–628 (1994).
9. H. Noji, H. Ueno, D. G. G. McMillan, Catalytic robustness and torque generation of the F<sub>1</sub>-ATPase. *Biophys. Rev.* **9**, 103–118 (2017).
10. H. Noji, R. Yasuda, M. Yoshida, K. Kinosita, Direct observation of the rotation of F<sub>1</sub>-ATPase. *Nature* **386**, 299–302 (1997).
11. T. Ariga, E. Muneyuki, M. Yoshida, F<sub>1</sub>-ATPase rotates by an asymmetric, sequential mechanism using all three catalytic subunits. *Nat. Struct. Mol. Biol.* **14**, 841–846 (2007).
12. R. Yasuda, H. Noji, K. Kinosita, M. Yoshida, F<sub>1</sub>-ATPase is a highly efficient molecular motor that rotates with discrete 120 degree steps. *Cell* **93**, 1117–1124 (1998).
13. R. Yasuda, H. Noji, M. Yoshida, K. Kinosita, H. Itoh, Resolution of distinct rotational substeps by submillisecond kinetic analysis of F<sub>1</sub>-ATPase. *Nature* **410**, 898–904 (2001).
14. K. Adachi *et al.*, Coupling of rotation and catalysis in F<sub>1</sub>-ATPase revealed by single-molecule imaging and manipulation. *Cell* **130**, 309–321 (2007).
15. T. Bilyard *et al.*, High-resolution single-molecule characterization of the enzymatic states in *Escherichia coli* F<sub>1</sub>-ATPase. *Philos. Trans. R. Soc. Lond. B Biol. Sci.* **368**, 20120023 (2013).
16. H. Noji *et al.*, Rotation of *Escherichia coli* F<sub>1</sub>-ATPase. *Biochem. Biophys. Res. Commun.* **260**, 597–599 (1999).
17. D. Spetzler *et al.*, Single molecule measurements of F<sub>1</sub>-ATPase reveal an interdependence between the power stroke and the dwell duration. *Biochemistry* **48**, 7979–7985 (2009).
18. H. Omote *et al.*, The  $\gamma$ -subunit rotation and torque generation in F<sub>1</sub>-ATPase from wild-type or uncoupled mutant *Escherichia coli*. *Proc. Natl. Acad. Sci. U.S.A.* **96**, 7780–7784 (1999).
19. D. Spetzler *et al.*, Microsecond time scale rotation measurements of single F<sub>1</sub>-ATPase molecules. *Biochemistry* **45**, 3117–3124 (2006).
20. R. Kobayashi, H. Ueno, C.-B. Li, H. Noji, Rotary catalysis of bovine mitochondrial F<sub>1</sub>-ATPase studied by single-molecule experiments. *Proc. Natl. Acad. Sci. U.S.A.* **117**, 1447–1456 (2020).
21. T. Suzuki, K. Tanaka, C. Wakabayashi, E.-i. Saita, M. Yoshida, Chemomechanical coupling of human mitochondrial F<sub>1</sub>-ATPase motor. *Nat. Chem. Biol.* **10**, 930–936 (2014).
22. B. C. Steel *et al.*, Comparison between single-molecule and X-ray crystallography data on yeast F<sub>1</sub>-ATPase. *Sci. Rep.* **5**, 8773 (2015).
23. J. Martin, R. Ishmukhametov, T. Hornung, Z. Ahmad, W. Frasch, Anatomy of F<sub>1</sub>-ATPase powered rotation. *Proc. Natl. Acad. Sci. U.S.A.* **111**, 3715–3720 (2014).
24. J. V. Bason, M. G. Montgomery, A. G. Leslie, J. E. Walker, How release of phosphate from mammalian F<sub>1</sub>-ATPase generates a rotary substep. *Proc. Natl. Acad. Sci. U.S.A.* **112**, 6009–6014 (2015).
25. L. Margulis, M. J. Chaplain, Endosymbioses: Cyclical and permanent in evolution. *Trends Microbiol.* **6**, 342–345 (1998).
26. J. J. García-Trejo *et al.*, The inhibitory mechanism of the  $\zeta$  subunit of the F<sub>1</sub>F<sub>0</sub>-ATPase nanomotor of *Paracoccus denitrificans* and related  $\alpha$ -Proteobacteria. *J. Biol. Chem.* **291**, 538–546 (2016).
27. J. A. Pérez, S. J. Ferguson, Kinetics of oxidative phosphorylation in *Paracoccus denitrificans*. 1. Mechanism of ATP synthesis at the active site(s) of F<sub>1</sub>F<sub>0</sub>-ATPase. *Biochemistry* **29**, 10503–10518 (1990).
28. F. Pacheco-Moisés, F. Minauro-Sanmiguel, C. Bravo, J. J. García, Sulfite inhibits the F<sub>1</sub>F<sub>0</sub>-ATP synthase and activates the F<sub>1</sub>F<sub>0</sub>-ATPase of *Paracoccus denitrificans*. *J. Bioenerg. Biomembr.* **34**, 269–278 (2002).
29. T. V. Zharova, A. D. Vinogradov, Proton-translocating ATP-synthase of *Paracoccus denitrificans*: ATP-hydrolytic activity. *Biochem. Biokhimiya* **68**, 1101–1108 (2003).
30. E. Morales-Rios *et al.*, A novel 11-kDa inhibitory subunit in the F<sub>1</sub>F<sub>0</sub> ATP synthase of *Paracoccus denitrificans* and related  $\alpha$ -proteobacteria. *FASEB J.* **24**, 599–608 (2010).
31. P. Serrano, M. Geraht, B. Mohanty, K. Wüthrich, NMR structures of  $\alpha$ -proteobacterial ATPase-regulating  $\zeta$ -subunits. *J. Mol. Biol.* **426**, 2547–2553 (2014).
32. M. Zarco-Zavala *et al.*, The  $\zeta$  subunit of the F<sub>1</sub>F<sub>0</sub>-ATP synthase of  $\alpha$ -proteobacteria controls rotation of the nanomotor with a different structure. *FASEB J.* **28**, 2146–2157 (2014).
33. E. Morales-Rios, M. G. Montgomery, A. G. Leslie, J. E. Walker, Structure of ATP synthase from *Paracoccus denitrificans* determined by X-ray crystallography at 4.0 Å resolution. *Proc. Natl. Acad. Sci. U.S.A.* **112**, 13231–13236 (2015).
34. A. Ludlam *et al.*, Chaperones of F<sub>1</sub>-ATPase. *J. Biol. Chem.* **284**, 17138–17146 (2009).
35. S. H. Ackerman, A. Tzagoloff, Identification of two nuclear genes (ATP11, ATP12) required for assembly of the yeast F<sub>1</sub>-ATPase. *Proc. Natl. Acad. Sci. U.S.A.* **87**, 4986–4990 (1990).
36. A. Picková, M. Potocký, J. Houstek, Assembly factors of F<sub>1</sub>F<sub>0</sub>-ATP synthase across genomes. *Proteins* **59**, 393–402 (2005).
37. F. Mendoza-Hoffmann *et al.*, The biological role of the  $\zeta$  subunit as unidirectional inhibitor of the F<sub>1</sub>F<sub>0</sub>-ATPase of *Paracoccus denitrificans*. *Cell Rep.* **22**, 1067–1078 (2018).
38. Y. Hirono-Hara *et al.*, Pause and rotation of F<sub>1</sub>-ATPase during catalysis. *Proc. Natl. Acad. Sci. U.S.A.* **98**, 13649–13654 (2001).
39. D. G. G. McMillan, R. Watanabe, H. Ueno, G. M. Cook, H. Noji, Biophysical characterization of a thermoalkaliphilic molecular motor with a high stepping torque gives insight into evolutionary ATP synthase adaptation. *J. Biol. Chem.* **291**, 23965–23977 (2016).
40. T. V. Zharova, A. D. Vinogradov, Energy-dependent transformation of F<sub>0</sub>F<sub>1</sub>-ATPase in *Paracoccus denitrificans* plasma membranes. *J. Biol. Chem.* **279**, 12319–12324 (2004).
41. H. Konno *et al.*, The regulator of the F<sub>1</sub> motor: Inhibition of rotation of cyanobacterial F<sub>1</sub>-ATPase by the epsilon subunit. *EMBO J.* **25**, 4596–4604 (2006).
42. K. Shimabukuro *et al.*, Catalysis and rotation of F<sub>1</sub> motor: Cleavage of ATP at the catalytic site occurs in 1 ms before 40 degree substep rotation. *Proc. Natl. Acad. Sci. U.S.A.* **100**, 14731–14736 (2003).
43. D. Okuno *et al.*, Correlation between the conformational states of F<sub>1</sub>-ATPase as determined from its crystal structure and single-molecule rotation. *Proc. Natl. Acad. Sci. U.S.A.* **105**, 20722–20727 (2008).
44. Y. Hirono-Hara, K. Ishizuka, K. Kinosita, M. Yoshida, H. Noji, Activation of pausing F<sub>1</sub> motor by external force. *Proc. Natl. Acad. Sci. U.S.A.* **102**, 4288–4293 (1995).
45. S. D. Dunn, R. G. Tozer, V. D. Zadorozny, Activation of *Escherichia coli* F<sub>1</sub>-ATPase by lauryldimethylamine oxide and ethylene glycol: Relationship of ATPase activity to the interaction of the epsilon and beta subunits. *Biochemistry* **29**, 4335–4340 (1990).
46. J.-M. Jault *et al.*, The  $\alpha_3\beta_3\gamma$  complex of the F<sub>1</sub>-ATPase from thermophilic *Bacillus PS3* containing the  $\alpha$ D261N substitution fails to dissociate inhibitory MgADP from a catalytic site when ATP binds to noncatalytic sites. *Biochemistry* **34**, 16412–16418 (1995).
47. H. R. Lotscher, C. DeJong, R. A. Capaldi, Interconversion of high and low ATPase activity forms of ECF<sub>1</sub> by the detergent lauryldimethylamine oxide. *Biochemistry* **23**, 4140–4143 (1984).
48. K. Hayashi, H. Ueno, R. Iino, H. Noji, Fluctuation theorem applied to F<sub>1</sub>-ATPase. *Phys. Rev. Lett.* **104**, 218103 (2010).
49. D. G. McMillan, S. Keis, P. Dimroth, G. M. Cook, A specific adaptation in the a subunit of thermoalkaliphilic F<sub>1</sub>F<sub>0</sub>-ATP synthase enables ATP synthesis at high pH but not at neutral pH values. *J. Biol. Chem.* **282**, 17395–17404 (2007).
50. P. D. Boyer, A perspective of the binding change mechanism for ATP synthesis. *FASEB J.* **3**, 2164–2178 (1989).
51. P. Mitchell, Molecular mechanics of protonmotive F<sub>0</sub>F<sub>1</sub> ATPases: Rolling well and turnstile hypothesis. *FEBS Lett.* **182**, 1–7 (1985).
52. T. M. Duncan, V. V. Bulygin, Y. Zhou, M. L. Hutcheon, R. L. Cross, Rotation of subunits during catalysis by *Escherichia coli* F<sub>1</sub>-ATPase. *Proc. Natl. Acad. Sci. U.S.A.* **92**, 10964–10968 (1995).
53. J. Weber, A. E. Senior, Bi-site catalysis in F<sub>1</sub>-ATPase: Does it exist? *J. Biol. Chem.* **276**, 35422–35428 (2001).
54. R. Watanabe *et al.*, Mechanical modulation of catalytic power on F<sub>1</sub>-ATPase. *Nat. Chem. Biol.* **8**, 86–92 (2011).
55. J. J. García, R. A. Capaldi, Unisite catalysis without rotation of the  $\gamma$ -c domain in *Escherichia coli* F<sub>1</sub>-ATPase. *J. Biol. Chem.* **273**, 15940–15945 (1998).
56. J. Pu, M. Karplus, How subunit coupling produces the  $\gamma$ -subunit rotary motion in F<sub>1</sub>-ATPase. *Proc. Natl. Acad. Sci. U.S.A.* **105**, 1192–1197 (2008).
57. C. B. Li, H. Ueno, R. Watanabe, H. Noji, T. Komatsuzaki, ATP hydrolysis assists phosphate release and promotes reaction ordering in F<sub>1</sub>-ATPase. *Nat. Commun.* **6**, 10223 (2015).
58. S. Mukherjee, A. Warshel, Dissecting the role of the  $\gamma$ -subunit in the rotary-chemical coupling and torque generation of F<sub>1</sub>-ATPase. *Proc. Natl. Acad. Sci. U.S.A.* **112**, 2746–2751 (2015).
59. H. Imamura *et al.*, Rotation scheme of V<sub>1</sub>-motor is different from that of F<sub>1</sub>-motor. *Proc. Natl. Acad. Sci. U.S.A.* **102**, 17929–17933 (2005).
60. H. Sielaff *et al.*, Power stroke angular velocity profiles of archaeal A-ATP synthase versus thermophilic and mesophilic F-ATP synthase molecular motors. *J. Biol. Chem.* **291**, 25351–25363 (2016).
61. Y. Minagawa *et al.*, Basic properties of rotary dynamics of the molecular motor *Enterococcus hirae* V<sub>1</sub>-ATPase. *J. Biol. Chem.* **288**, 32700–32707 (2013).
62. S. Furuike *et al.*, Resolving stepping rotation in *Thermus thermophilus* H<sup>+</sup>-ATPase/synthase with an essentially drag-free probe. *Nat. Commun.* **2**, 233 (2011).
63. T. Iida *et al.*, Single-molecule analysis reveals rotational substeps and chemo-mechanical coupling scheme of *Enterococcus hirae* V<sub>1</sub>-ATPase. *J. Biol. Chem.* **294**, 17017–17030 (2019).
64. H. Noji, H. Ueno, R. Kobayashi, Correlation between the numbers of rotation steps in the ATPase and proton-conducting domains of F- and V-ATPases. *Biophys. Rev.* **12**, 303–307 (2020).
65. I. Watt, M. Montgomery, M. Runswick, A. Leslie, J. Walker, Bioenergetic cost of making an adenosine triphosphate molecule in animal mitochondria. *Proc. Natl. Acad. Sci. U.S.A.* **107**, 16823–16827 (2010).
66. H. Guo, T. Suzuki, J. L. Rubinstein, Structure of a bacterial ATP synthase. *eLife* **8**, e43128 (2019).
67. M. Sobti *et al.*, Cryo-EM structures of the autoinhibited *E. coli* ATP synthase in three rotational states. *eLife* **5**, e21598 (2016).

68. W. C. Y. Lau, J. L. Rubinstein, Structure of intact *Thermus thermophilus* V-ATPase by cryo-EM reveals organization of the membrane-bound  $V_o$  motor. *Proc. Natl. Acad. Sci. U.S.A.* **107**, 1367–1372 (2010).
69. T. Murata, I. Yamato, Y. Kakinuma, A. G. W. Leslie, J. E. Walker, Structure of the rotor of the V-type  $\text{Na}^+$ -ATPase from *Enterococcus hirae*. *Science* **308**, 654–659 (2005).
70. T. Meier, P. Polzer, K. Diederichs, W. Welte, P. Dimroth, Structure of the rotor ring of F-Type  $\text{Na}^+$ -ATPase from *Ilyobacter tartaricus*. *Science* **308**, 659–662 (2005).
71. S. Saroussi, M. Schushan, N. Ben-Tal, W. Junge, N. Nelson, Structure and flexibility of the C-ring in the electromotor of rotary  $F_oF_1$ -ATPase of pea chloroplasts. *PLoS One* **7**, e43045 (2012).
72. D. Pogoryelov, Ö. Yildiz, J. D. Faraldo-Gómez, T. Meier, High-resolution structure of the rotor ring of a proton-dependent ATP synthase. *Nat. Struct. Mol. Biol.* **16**, 1068 (2009).
73. L. Preiss *et al.*, Structure of the mycobacterial ATP synthase  $F_o$  rotor ring in complex with the anti-TB drug bedaquiline. *Sci. Adv.* **1**, e1500106 (2015).
74. F. Varghese, J. N. Blaza, A. J. Y. Jones, O. D. Jarman, J. Hirst, Deleting the IF<sub>1</sub>-like  $\zeta$  subunit from *Paracoccus denitrificans* ATP synthase is not sufficient to activate ATP hydrolysis. *Open Biol.* **8**, 170206 (2018).
75. M. Zarco-Zavala, F. Mendoza-Hoffmann, J. J. García-Trejo, Unidirectional regulation of the  $F_1F_o$ -ATP synthase nanomotor by the  $\zeta$  pawl-ratchet inhibitor protein of *Paracoccus denitrificans* and related  $\alpha$ -proteobacteria. *Biochim. Biophys. Acta Bioenerg.* **1859**, 762–774 (2018).
76. D. J. Klionsky, W. S. Brusilow, R. D. Simoni, *In vivo* evidence for the role of the epsilon subunit as an inhibitor of the proton-translocating ATPase of *Escherichia coli*. *J. Bacteriol.* **160**, 1055–1060 (1984).
77. R. Watanabe, R. Iino, H. Noji, Phosphate release in  $F_1$ -ATPase catalytic cycle follows ADP release. *Nat. Chem. Biol.* **6**, 814–820 (2010).